Kirchhoff diffractals

1994 J. Phys. A: Math. Gen. 27 5979

(http://iopscience.iop.org/0305-4470/27/17/029)

J. Phys. A: Math. Gen. 27 (1994) 5979–5993. Printed in the UK

Kirchhoff diffractals

O I Yordanov and K Ivanova

Bulgarian Academy of Sciences, Institute of Electronics, boul. 'Tzarigradsko shoussee' 72, Sofia 1784, Bulgaria

Received 14 February 1994

Abstract. We study the angular properties of plane waves backscattered from random fractal curves and surfaces (diffractals). For this purpose we apply the physical optics (Kirchhoff) approximation without resorting to the high-frequency limit. The fractals of interest are described by Gaussian random processes possessing power-law spectra with and without a large-scale cut-off. We show that if the wavelength of the incident field is of order of the topothesy, small variations of its value may alter the angular pattern of the backscattered power qualitatively. The most important prediction is a peak which Kirchhoff diffractals exhibit under specific conditions at a particular angle of incidence. The position of the peak is linked to the dimension of the topothesy and provides a good possibility for experimental measurement of these intrinsic parameters of the fractal surfaces. The effect of large-scale cut-off which determines the RMS height of the surface is also studied.

1. Introduction

We are concerned in this paper with scattering of scalar waves by Gaussian random rough curves and surfaces which possess irregularities over a wide range of scales. More specifically, we consider isotropic surfaces described by simple power-law roughness spectra

$$S_1(q) = A_1 q^{-\alpha} \tag{1.1}$$

with and without large-scale cut-off. Above, A_1 is the spectral constant and the parameter α is assumed to take values in the interval $D_T < \alpha < D_T+2$; D_T denotes the usual topological dimension, $D_T = 1$ for curves and $D_T = 2$ for surfaces; q designates either $|k|$, for $D_T = 1$ or $|k_\perp|$ ($k_\perp = (k_x, k_y)$), for $D_T = 2$. These types of spectra are known to give rise to fractal curves and surfaces, i.e. curves and surfaces with hierarchical structure characterized with statistical self-similarity [1]. Since the publication of [2], fractals have been the focus of interest for various physical disciplines, proving to be pertinent models for a variety of physical phenomena; the reader may refer, for example, to [3]. In particular, the type of fractal models considered here apply to a wide class of surfaces; see the experimental data collected in: [4] related to terrain and some man-made surfaces; [5]—ocean surface; [6]—ocean bottom; [7]—the surface of the Moon; [8]—fracture surfaces etc.

In the next section we discuss, in detail, the structure functions associated with (1.1) and the parameters which govern their behaviour: these are the Hausdorff–Besicovitch dimension [9], the topothesy [4] and the RMS height. The discussions emphasize the insight which fractal geometry provides for understanding the properties of the random surfaces.

Studying the scattering by fractal surfaces, similar to Berry and Blackwell [10], we employ the physical optics, or Kirchhoff tangent plane approximation. (Waves that have

0305-4470/94/175979+15$19.50

encountered fractals have been called diffractals by Berry; hence, the term Kirchhoff diffractals used as the title of this paper.) However, rather than an incident Gaussian beam we consider an incident plane wave, and rather than the late-time echo tail decay we focus on the angular dependence of the scattered intensity. Another difference is our assumption that both the source and the receiver reside in the far, Fraunhofer zone. It is argued in section 3, that the conditions ensuring the Fraunhofer zone approximation are usually satisfied if the wavelength of the diffractal is sufficiently small. On the other hand, if the wavelength is not small, the far zone approximation is still a reasonable assumption provided the dimension of the surface does not exceed a specific value.

Since the high-frequency approximation is not applicable to scattering from fractal structures [1, 11], for the evaluation of the scattering cross section we employ an elaborated combination of numerical and asymptotic techniques. The technique allows evaluation of the scattering cross section for any set of surface and scattering parameters. Details of this technique, not discussed in our earlier publications, are presented in section 4.

In section 5, we present numerical results which reveal some of the characteristics of the considered diffractals and the conditions under which the diffractal regime comes into effect. Special attention is paid to wavelengths close to the surface topothesy. A new critical type behaviour, which we call diversification of the angular diffractal patterns is predicted. The impact of the large-scale cut-off is also studied in this section. A summary of the obtained results is presented in the last section.

2. Random curves and surfaces with power-law spectra

We shall refer to type I, or 'pure' fractal surfaces, if the surface has a spectrum of the form of (1.1) with no spectral cut-offs, and to type II surfaces, for spectra with an absolutely sharp large-scale cut-off k_a; i.e.

$$S_{II}(q) = \begin{cases} A_{II} q^{-\alpha} & q \geqslant k_a \\ 0 & q < k_a . \end{cases} \tag{2.1}$$

It should be stressed that by considering roughness spectra of the form (1.1) and (2.1) we actually restrict our study to isotropic curves and surfaces.

From the standpoint of fractal geometry, the most important characteristic of both types of surfaces is the Hausdorff–Besicovitch, or fractal, dimension D. It has been shown [9, 1] that the dimension of a type I fractal curve is related solely to the exponent α. This is done by using the 'potential' definition of the fractal dimension [2]. By calculating the energy of a uniformly charged surface defined over a circular region, the same can easily be demonstrated for the case of $D_T = 2$, for both type I and II surfaces. Denoting the excess of the fractal dimension over the topological dimension by $D' = D - D_T$, the relation which links the fractal dimension to α can be written in the following unified for both $D_T = 1$ and $D_T = 2$ form

$$D' = (D_T + 2 - \alpha)/2 . \tag{2.2}$$

Clearly $0 < D' < 1$ when $D_T < \alpha < D_T + 2$. For the assumed values of the spectral exponent, the Fourier transform of S_I is a divergent integral; thus, the correlation function does not exist. Similarly, the RMS height, and therefore, the RMS slope are infinity. However, the so-called structure, or mean-square increment (MSI), function defined by

$\Delta_I(\xi) = \langle(\zeta(\xi_0 + \xi) - \zeta(\xi_0))^2\rangle$ (the broken brackets denote ensemble average) does exist and is given by [1]

$$\Delta_I(\xi) = \tau_I^{2D'}\xi^{2(1-D')}. \tag{2.3}$$

Here ξ denotes $|x|$ in the case of $D_T = 1$ and $|r_\perp|$ ($r_\perp = (x, y)$), in the case of $D_T = 2$. The important parameter τ_I, termed topothesy, is by definition, the distance over which the MSI function equals τ_I^2. The following relationship expresses the topothesy in terms of the parameters A_I and D' (or equivalently in A_I and α):

$$\tau_I^{2D'} = \frac{A_I 2^{2D'-D_T-1}\Gamma(D')}{\pi^{D_T/2}(1 - D' + D_T/2)}. \tag{2.4}$$

As we shall see in the next sections, the parameter τ_I plays a key role in assessing the characteristics of the waves that have encountered fractals. At both limiting cases $D' \to 0$ and $D' \to 1$ called marginal and extreme fractals, respectively, the topothesy tends to infinity. Another special case is $D' = \frac{1}{2}$, called, in analogy with the Brownian motion, Brownian fractal surfaces, for which (2.3) and (2.4) simplify to $\Delta_I(\xi) = \tau_I\xi$, $\tau_I = A_I/\pi^{D_T-1}$. The dependence of τ_I upon the dimension D' is graphically illustrated in [12, 13].

Since the behaviour of $S_I(q)$ and $S_{II}(q)$ for large q are identical, the MSI functions $\Delta_I(\xi)$ and $\Delta_{II}(\xi)$ must behave identically at zero. Indeed, calculating the structure function corresponding to (2.1) (see appendix A) one obtains

$$\Delta_{II}(\xi) = \tau_{II}^{2D'}\xi^{2(1-D')} + 2h^2\left[1 - {}_1F_D', D_T/2; -k_a^2\xi^2/4)\right] \tag{2.5}$$

where τ_{II} is given by the same expression (2.4); hence, thereafter we suppress the subscripts of the topothesy. Equation (2.5) involves the hypergeometric function ${}_1F_2$; since it is an entire function, (2.5) defines $\Delta_{II}(\xi)$ for arbitrary ξ. At $\xi \to 0$, ${}_1F_2$ approaches unity and therefore $\Delta_{II}(\xi) \sim \Delta_I(\xi)$, as $\xi \to 0$. Type II spectra have finite RMS height h and infinite RMS slope. In terms of the spectral parameters, the RMS height reads

$$h^2 = \frac{A_{II}k_a^{2(D'-1)}}{2\pi D_T(1 - D')}. \tag{2.6}$$

As expected $h \to \infty$ as $k_a \to 0$. Due to high-frequency divergence, the RMS height grows unbounded as Hausdorff–Besicovitch dimension approaches the extreme fractal case.

After sharp increase for small and intermediate ξ, type II structure functions approach $2h^2$ at infinity in an oscillatory fashion (the amplitude of the oscillations decrease with increasing D'). The leading asymptotic term of $\Delta_{II}(\xi)$ for large ξ is given by

$$\Delta_{II}(\xi) \sim 2h^2\left[1 + \frac{2(1 - D')}{k_a\xi}\begin{Bmatrix}\sin(k_a\xi)\\ J_1(k_a\xi)\end{Bmatrix}\right] \qquad \begin{Bmatrix} D_T = 1\\ D_T = 2\end{Bmatrix} \tag{2.7}$$

where J_1 is the first-order Bessel function. The last expression provides another characteristic length—the distance which separates the scales of fractality from the scales of 'geography' [10]. From (2.7), the type II structure function is close to $2h^2$ for values of its argument much greater than L, where

$$L = 2\pi^{(1-D_T)/3}(1 - D')^{(4-D_T)/3}k_a^{-1}. \tag{2.8}$$

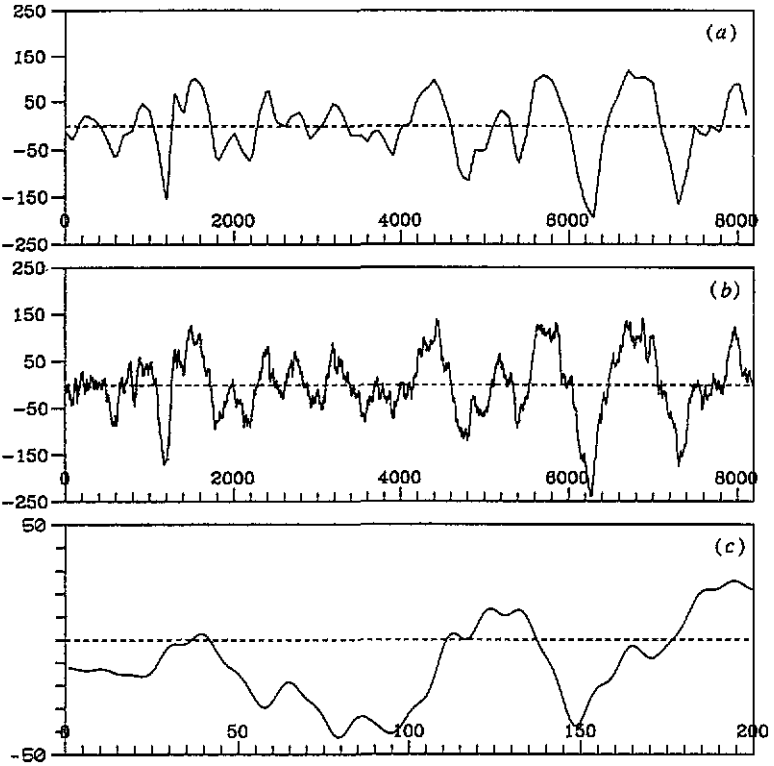

Figure 1. Simulated random fractal profile for parameters: dimension $D = 1.25$, topothesy $\tau = 10\Delta x$, RMS height $h = 50\Delta x$. The discretization step is $\Delta x = 1$ (arbitrary units), the total number of points is $N_p = 8192$. In (a) the profile is drawn with resolution $100\Delta x$; in (b) with resolution Δx; in (c) a magnified portion of the surface consisting of the first 200 points is shown.

Graphs of $\Delta_\Pi(\xi)$ labelled by different values of the fractal dimension are drawn in [12].

A physically realistic spectrum must also have a small-scale cut-off k_b. The presence of such a cut-off makes a surface with a finite domain power-law spectrum an ordinary, rectifiable [14] surface (when viewed at very fine resolutions). The Hausdorff–Besicovitch dimension for such surfaces equals the topological dimension, $D = D_T$. Nonetheless, the surfaces exhibit an approximate self-similarity over a wide range of horizontal distances [15]. The Hausdorff–Besicovitch dimension is then substituted by the similarity dimension D_S [16], whose excess over D_T is given to a good approximation by (2.2). Hence, in most of the cases, the effect of the small-scale cut-off can be minimized by choosing the wavelength of the incident field well within the self-similarity range. Only when α is close to D_T, the existence of small-scale cut-off essentially changes the overall self-similar behaviour [15], and in this case, one should expect essential impact of k_b on the diffractal properties as well. This impact, however, will not be pursued here.

We conclude this section with illustrations of power-law surface realizations which provide an insight into the expected diffractal properties. The surfaces are simulated using an algorithm described in [17, 18] choosing discretization step of $\Delta x = 1$ (in arbitrary units) and total number of points $N_p = 8192$. For the surface in figure 1, we prescribed $D = 1.25$, $\tau = 10\Delta x$, $h = 50\Delta x$. In figure 1(a) the surface is drawn with a resolution of 10τ. At this resolution the fractal surface appears similar to an ordinary, non-fractal

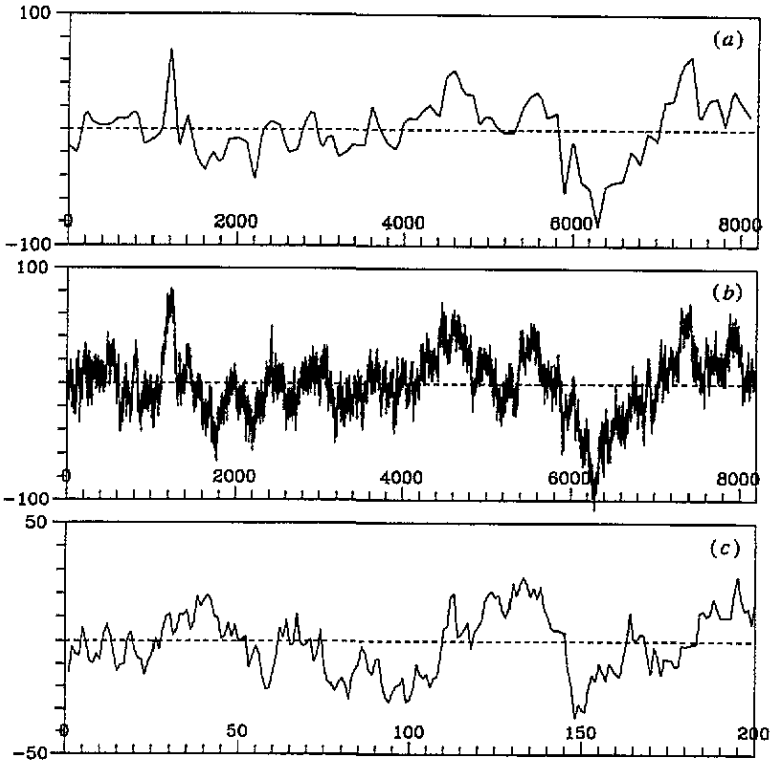

Figure 2. The same as figure 1, except that $D = 1.75$ and $h = 20\Delta x$.

surface—see figure 2 in [19]—with an effective slope defined by $s_{\text{eff}} = \sqrt{2}h/L$, where L is given by (2.8). For the parameters of figure 1, $s_{\text{eff}} = 0.188$. Therefore, when illuminated by a wave with wavelength $\lambda \gg \tau$, the returns from a fractal surface should be qualitatively similar to that of a non-fractal one. In figure 1(b) the same surface is drawn with resolution 0.1τ. A great number of new rough patches are seen whose average size is of order of τ; cf with the graphs of the Weierstrass–Mandelbrot fractal function given in [20]. If $\lambda \lesssim \tau$ the contribution to the scattered power from small scale roughness should be dominant. The mean slope of this roughness is visibly greater than 0.188, see figure 1(c), in which a magnified portion consisting of the first 200 points is shown. (We should note, that the computer realizations actually do have a small-scale cut-off demanded by the Nyquist frequency, in our case $k_b = \pi$.) On the other hand, according to the predictions of the geometric optics, the backscattered power from a Gaussian correlated surface with a steep slope $s > \sqrt{2 + D_T}$, exhibits a peak at a certain angle of incidence. Thus, a similar peak should be expected in the backscatter from a fractal surface power for $\lambda \lesssim \tau$.

Figure 2 shows realization of a random fractal surface with the same parameters except that $D = 1.75$ and $h = 20$. In this case, at resolution 10τ—figure 2(a)—the effective slope is $s_{\text{eff}} = 0.056$. However, at resolution 0.1τ, the fractality scales are rougher—figure 2(b), and steeper—figure 2(c). Therefore, the maximum of the backscattered power should be expected at about grazing incidence.

3. Physical optics approximation

Both classical methods in the theory of scattering by rough surfaces—small perturbations and Kirchhoff approximations—have been applied to fractal surfaces. The Born approximation has been used by Po-zen Wong [21] to derive the asymptotic form of the Fourier transform of the scatter from porous solids with fractal interface intensity. However, there are no known criteria for validity of the ordinary perturbation techniques [22, 23] when applied to scattering from fractal surfaces. As a recent Monte Carlo simulations show [24] even in the case of single-scale Gaussian correlated one-dimensional surfaces, the requirement $\hat{h} \equiv kh \ll 1$ (k is the wavenumber of the incident field) does not suffice to ensure the validity of the first-order perturbation approximation. (It must be supplemented with a certain small-correlation-length condition.)

Since the Kirchhoff approximation is a heuristic rather than an asymptotic method (based on the local tangent-plane approximation), the question of its applicability for description of diffractal scattering is even more difficult to address. (It is true that the Kirchhoff approximation has also been shown to be the zero-order iterative solution of the surface field integral equation [25, 26]. However, the conditions for convergency of the iterative series are not known, and moreover, even what parameter should be considered as small for this expansion depends on the statistical parameters of the surface [27, 28].) To appreciate the difficulties in defining an appropriate parameter, controlling the accuracy of the Kirchhoff approximation, the reader may refer to the paper by Thorsos [19] where the widely accepted criteria—large radius of curvature compared to the wavelength [29]—was tested in Monte Carlo simulations, again for Gaussian correlations, and found inappropriate. Instead, the criterion $l_{corr} \geqslant \lambda$ has been suggested for all scattering directions away from grazing; l_{corr} is the correlation length and λ is the wavelength of the incident field. (See also, [28] where detailed criteria based on a variational correction to the Kirchhoff approximation are derived. In these criteria l_{corr}/λ is involved as a key parameter.) By analogy, one may expect that for wavelengths of order or less than topothesy the Kirchhoff diffractals, at least qualitatively, would give a proper picture of the scattering. On the other hand, if the wavelength is much greater than topothesy, the scales of fractality, as we shall see, have negligible effect on the scattered field. In this case the surface can be regarded as a non-fractal rough surface with criterion for validity of the Kirchhoff approximation $L/\lambda \geqslant 1$, see equation (2.8).

Let us also note the studies [7] and [30] where the scattering from power-law surfaces is considered in the framework of the two-scale model—a combination of physical optics and perturbation expansion [22]. Finally, the problem of scattering from type I surfaces for the particular case of fractal dimension $D = 2.25$ has recently been treated in an approach that requires the surface slopes to be small [31].

Before proceeding further, we elaborate on the conditions validating the far (Fraunhofer) zone approximation adopted throughout this paper. For non-fractal rough surfaces these conditions are obtained, for example, in [32] and studied in detail in [33]. According to the analysis carried out for fractal surfaces in [34], the source/receiver is located in the far zone if its distance R from the fractal surface satisfies the condition

$$R \gg R_F = b \cos\theta_i \left(\frac{1}{k\tau \cos\theta_i} \right)^{D'/(1-D')} \tag{3.1}$$

where b is the size of the illuminated area and θ_i is the angle of incidence measured from the vertical, z-axis. Independent of the value of the fractal dimension, the condition (3.1) is easily satisfied provided $\lambda \leqslant 2\pi\tau \cos\theta_i$. In the case of longer probing waves, the

Fraunhofer-type scattering is in effect for surfaces having dimensions for which

$$D' < \left[1 + \frac{\ln(1/\hat{\tau}\cos\theta_i)}{\ln(R/b\cos\theta_i)}\right]^{-1} \tag{3.2}$$

where the dimensionless topothesy $\hat{\tau} = k\tau$ is introduced.

Assuming that inequality (3.1) holds, one can make use of the definition of the dimensionless incoherent scattering cross section per unit area per unit scattered solid angle, see, for example, [35, 19],

$$\sigma(\boldsymbol{k}_s, \boldsymbol{k}_i) = \left(\frac{k}{\pi}\right)^{D_T-1}\frac{q^4}{q_z^2}\int d^{D_T}\boldsymbol{r}_\perp e^{i\boldsymbol{q}_\perp\boldsymbol{r}_\perp}\left[\exp\left(-\frac{q_z^2}{2}\Delta(|\boldsymbol{r}_\perp|)\right) - \exp\left(-q_z^2h^2\right)\right]. \tag{3.3}$$

The above expression pertains to a scattering from a surface with infinite extent. The wavevector of the incident plane wave is $\boldsymbol{k}_i = k(\sin\theta_i, 0, -\cos\theta_i)$, the direction of the scattering is determined by $\boldsymbol{k}_s = k(\sin\theta_s\cos\varphi, \sin\theta_s\sin\varphi, \cos\theta_s)$; by definition $\boldsymbol{q} = (\boldsymbol{q}_\perp, q_z) = \boldsymbol{k}_i - \boldsymbol{k}_s$. (We remark that for type I surfaces the second term in the integrand of (3.3)—that is the coherent part of the intensity—vanishes.) Making use of the isotropy of the surface, the expression for the scattering cross section is brought to the following convenient form:

$$\sigma(\boldsymbol{k}_s, \boldsymbol{k}_i) = \frac{\hat{q}^4}{2\hat{q}_z^2(|\hat{q}_z|\hat{\tau}^{D'})^{D_T/(1-D')}}\int_0^\infty du\begin{Bmatrix}\cos(pu)\\ uJ_0(pu)\end{Bmatrix} \times\left[\exp\left(-\tfrac{1}{2}\hat{\Delta}(u)\right) - \exp\left(-\hat{q}_z{}^2\hat{h}^2\right)\right] \qquad \begin{cases} D_T = 1\\ D_T = 2\end{cases} \tag{3.4}$$

where the (dimensionless) parameters $\hat{q} = q/k$, and $p = |\hat{q}_\perp|/(|\hat{q}_z|\hat{\tau}^{D'})^{1/(1-D')}$ are introduced. The dimensionless type I and type II structure functions are defined by $\hat{\Delta}_I(u) = u^{2(1-D')}$ and $\hat{\Delta}_{II}(u) = u^{2(1-D')} + 2q_z^2h^2\left(1 - {}_1F_2\left(D' - 1;\ D',\ D_T/2;\ -\tilde{k}_a^2u^2/4\right)\right)$, respectively, with $\tilde{k}_a = \hat{k}_a/(|\hat{q}_z|\hat{\tau}^{D'})^{1/(1-D')}$. Equation (3.4) can be numerically implemented to yield values of $\sigma(\boldsymbol{k}_i, \boldsymbol{k}_s)$ for any set of scattering and surface statistical parameters, except, as we shall see later, those for which the parameter p is large. For the case of pure fractal surfaces, however, it is instructive to develop a series representation of the scattering cross section. This representation, as well as an asymptotic expansion of (3.4) for large p, are obtained in the next section.

4. Series representations and asymptotic expansions of the scattering cross section

The key to the series representation of $\sigma(\boldsymbol{k}_s, \boldsymbol{k}_i)$ for type I surfaces is the integral

$$B(p, D'; D_T) = \int_0^\infty\begin{Bmatrix}\cos(pu)\\ uJ_0(pu)\end{Bmatrix}\exp\left(-\tfrac{1}{2}u^{2(1-D')}\right)du \qquad \begin{cases} D_T = 1\\ D_T = 2.\end{cases} \tag{4.1}$$

Two cases should be distinguished. If $D' < \frac{1}{2}$, a convergent series is obtained from (4.1) by simply expanding the oscillatory functions and integrating term by term. Referring, for example, to [36] the result is

$$B(p, D'; D_T) = \frac{\Gamma(D_T/2)}{2(1-D')}\sum_{n=0}^{\infty}(-1)\frac{2^{(n+D_T/2)/(1-D')}\Gamma((n + D_T/2)/(1 - D'))}{2^{2n}\,n!\,\Gamma(n + D_T/2)}p^{2n}. \tag{4.2}$$

The case $D' > \frac{1}{2}$ requires more effort. Let us take, for example, $D_T = 2$ and consider the complex integral

$$\int_0^\infty z H_0^{(1)}(pz) \exp\left[-\tfrac{1}{2}(z)^{2(1-D')}\right] dz \tag{4.3}$$

with a branch cut along the positive real axis. The integrand of (4.3) involves the first kind, zero-order Hankel function $H_0^{(1)}$; the values of $Z^{2(1-D')}$ are defined in such a way that $B(p, D'; 2)$ is obtained by taking the real part of (4.3). Using this, a series representation is developed by deforming the integration contour to the positive imaginary axis and expanding the exponent. A similar technique can be applied for topological dimension $D_T = 1$, render

$$B(p, D'; D_T) = \frac{D_T}{(\sqrt{\pi}\, p)^{D_T}} \times \sum_{n=1}^{\infty} (-1)^{n+1} \frac{[n(1-D')]!\Gamma[n(1-D') + D_T/2] \sin[n\pi(1-D')]}{n! 2^{n(2D'-1)} p^{2n(1-D')}} \tag{4.4}$$

which is convergent for $D' > \frac{1}{2}$. We note, that in a different physical context, a series with essentially the same structure has been obtained by Berry and Blackwell [9], and also for the particular case of $D' = \frac{1}{4}$ in [31].

In practice, the evaluation of $B(p, D'; D_T)$ from the series representation is limited by the computer precision. The 'radius of effective numerical convergence' for (4.2) can be prescribed by

$$p \leqslant p_< = \left(\frac{1+2\eta}{2}\right)^{1/(1+2\eta)} \left(\frac{1+2\eta}{2\eta} M \ln 10\right)^{2\eta/(1+2\eta)} \tag{4.5}$$

where $\eta = \frac{1}{2} - D'$, and M is the maximum number of digits not rounded off by the computer. Alternatively, for $D' = \frac{1}{2} + \eta$, $0 < \eta < \frac{1}{2}$ the series (4.4) converges numerically provided

$$p \geqslant p_> = \left(\frac{1-2\eta}{2}\right) \left(\frac{\eta}{M \ln 10}\right)^{2\eta/(1-2\eta)}. \tag{4.6}$$

The series representations are computationally more efficient and reliable than the direct numerical integration of (3.4), provided the surface dimension is not close to $D_T + \frac{1}{2}$. If $\eta \ll 1$, i.e. the surface is similar to a Brownian fractal, the intervals of convergence are the narrowest; also the rate of convergence of (4.2) and (4.4) is extremely slow. On the other hand, for the cases in which (4.2) and (4.4) are not convergent—i.e. for $D' > \frac{1}{2}$ and $D' < \frac{1}{2}$, respectively—they represent full asymptotic expansions of $B(p, D'; D_T)$. Thus, in the actual evaluation of the scattering cross section, the representation (4.2) can be used for small p whilst (4.4) for large p independent of the value of the fractal dimension D. When $B(p, D'; D_T)$ is calculated from an asymptotic series, the so-called optimal truncation rule [37] has proved, in our experience, to be always reliable. The absolute errors of the asymptotic summation are given by

$$E(\eta) = \frac{1}{\sqrt{2\pi}} \exp\left[-\eta \left(\frac{1-2\eta}{2p}\right)^{(1-2\eta)/2\eta}\right] \tag{4.7}$$

for equation (4.2), and

$$E(\eta) = \sqrt{2\pi}\exp\left[-\eta\left(\frac{2p}{1+2\eta}\right)^{(1+2\eta)/2\eta}\right] \tag{4.8}$$

for equation (4.4). As it is seen from (4.8), for fixed η and large values of p, the error of the asymptotic summation is reasonably small allowing the handling of this most difficult numerical integration case, see below.

The case of pure Brownian fractal curves and surfaces permits an exact quadrature of (4.1) leading to the following simple expression:

$$B\left(p, \tfrac{1}{2}, D_T\right) = \frac{2D_T}{(1+4p^2)^{(1+D_T)/2}}. \tag{4.9}$$

We remark that for $D' = \frac{1}{2}$, both (4.2) and (4.4) can formally be summed up with a result (4.9).

We now turn to the problems involved in the practical evaluation of (3.4) for type II surfaces. For this purpose we use numerical quadrature for small and intermediate values of p. To control the error, we break the interval of integration into subintervals in which the integrand is either positive or negative. (In the case of $D_T = 2$, these intervals are defined by $(j_{0,n}, j_{0,n+1})$, where $j_{0,n}$ and $j_{0,n+1}$ are two consecutive zeroes of the Bessel function J_0. As is often the case, large numbers of subintervals have to be accounted for; to calculate $j_{0,n}$ for large n, the asymptotic expression for the zeroes has been used [38].) It has been observed that series generated by the values of the integral over the subintervals behaves, in general, as an asymptotic series. Hence, the summation is carried out using error control rules of asymptotic series [37].

With increasing p, the numerical error becomes intolerable. Special difficulties present the case of extreme fractal surfaces, when the rapid oscillations are imposed on an extremely slow decrease of the non-oscillating factors in the integrand of (3.4). To handle these cases, we develop a full asymptotic expansion of $\sigma(k_s, k_i)$ using p as a large parameter.

When p is large the main contribution to the integral comes from the vicinity of $u = 0$. However, no ordinary asymptotic technique can be applied for the estimation of this contribution. The remedy is a special technique developed in [39]. It employs the Parseval relation for the Melin transforms of the oscillating and non-oscillating factors of (3.4). Not presenting the long and rather cumbersome calculations, we write down only the final expansion. If for some integer M an error less than $(p/2)^{-2(1-D')M}$ is desired, the asymptotic form of the scattering cross section for large p reads

$$\sigma(k_i, k_i) = \frac{\Gamma(D_T/2)\hat{q}^4}{2\hat{q}_z^2(|\hat{q}_z|\hat{\tau}^{D'})^{D_T/(1-D')}}\left(\frac{p}{2}\right)^{-D_T}\sum_{m=1}^{M}\frac{(-1)^m}{2^{m+1}} \times \sum_{0\leqslant k_1+\cdots+k_N<m}\frac{A_1^{k_1}A_2^{k_2}\ldots A_N^{k_N}\Gamma((D_T+\mu)/2)}{k_1!\,k_2!\ldots k_N!\,(m-k_1-\cdots-k_N)!\,\Gamma(-\mu/2)}\left(\frac{p}{2}\right)^{-\mu} \tag{4.10}$$

where

$$A_n = (-1)^n\frac{(2\hat{q}_z^2\hat{h}^2)(1-D')\Gamma(D_T/2)}{(D'+n-1)\Gamma(D_T+n)n!}\left(\tfrac{1}{4}\tilde{k}_a^2\right)^n$$

and $\mu = \mu(m, k_1, \ldots, k_N) = 2(1 - D')(m - k_1 - \cdots - k_N) + 2\sum_{l=1}^{N} l\,k_l$. The second summation in (4.10) is over all possible sets of integers $k_1, \ldots, k_N$ whose sum is less than m. Complying with the error bound, the sets $k_1, \ldots, k_n$ for which $\mu > 2(1 - D')M$ must be suppressed. Note that the leading order in (4.10) does not depend on the RMS height and is identical with the large p leading order for type I surfaces (obtained by accounting for the term with $n = 1$ in (4.4) only). Hence, with increasing p the predictions of (3.4) are insensitive to the value of largest scale.

To conclude this section, we stress that, in our experience, the evaluation of quantities which characterize the diffractal properties, calls for a careful numerical work and often accounting for pertinent full asymptotic expansions.

5. Backscattered diffractal patterns

We begin our exposé of the properties of the backscattered Kirchhoff diffractals with the main finding of this work. Figure 3 shows backscattering cross section, $\sigma_B(\theta_i)$—equation (3.4) with $\theta_i = -\theta_s$—as a function of the angle of incidence for three values of the wavelength, all of them close to the topothesy's length. The full curves represent $\sigma_B(\theta_i)$ for type II surfaces with $h/\lambda = 1.59$, whereas the dotted curves correspond to 'pure diffractals', i.e. with $h/\lambda = \infty$. The fractal dimension used to produce the data for figure 1 is $D = 2.3$. For backscattering, large angles of incidence lead to large values of p, and as expected, the values of σ_B for type I and type II surfaces merge with increasing θ_i. The first two curves are plotted using dimensionless topothesy of $\hat{\tau} = 0.2$ ($\tau/\lambda = 0.032$) and have a form which is typical for scattering from non-fractal surfaces: a maxima at $\theta_i = 0$ and a minima as the angle of incidence approaches grazing. When the wavelength is decreased below a specific value, the backscattered pattern change qualitatively; namely, the curves

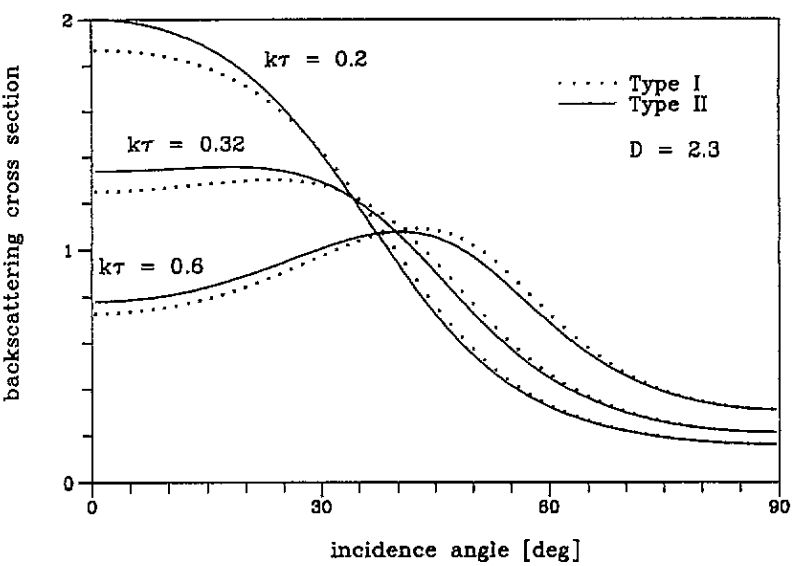

Figure 3. Backscattering diffractal patterns for dimension of the surface $D = 2.3$. The full curves correspond to type II surfaces with dimensionless RMS height $\hat{h} = kh = 10$, the dotted—to type I surface—$\hat{h} = \infty$. The values of the dimensionless topothesy $\hat{\tau} = k\tau$ used to produce the different curves are given inside the figure.

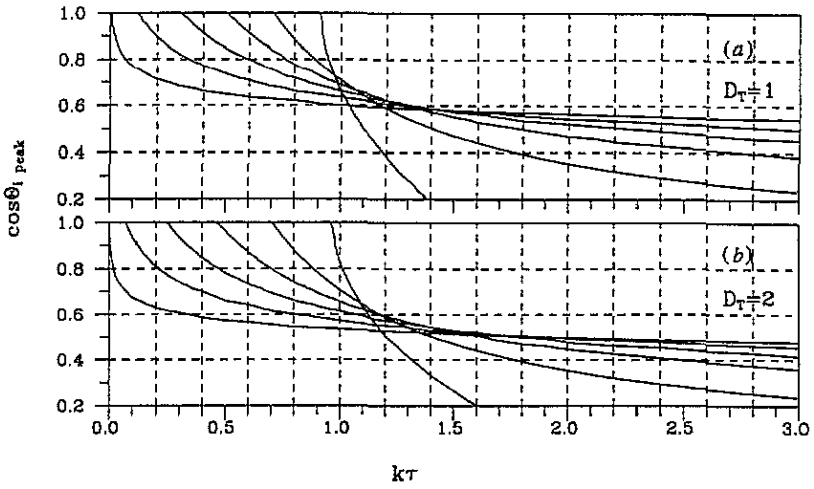

Figure 4. Cosine of θ_{ipeak} versus the dimensionless topothesy for type I surfaces and (*a*) $D_T = 1$, (*b*) $D_T = 2$. The graphs correspond to excesses of the fractal dimension of $D' = 0.1, 0.2, 0.3, 0.4, 0.5$, and 0.6, respectively from left to right.

marked with $\hat{\tau} = 0.32$ ($\tau/\lambda = 0.051$) exhibit minima at normal and grazing incidence, and mild maximum at about $\theta_i = 20°$ for type II surfaces, and at about $\theta_i = 28°$ for the pure fractal case. With further decrease of the wavelength the peak becomes more pronounced; see the pair of curves corresponding to $\hat{\tau} = 0.6$ ($\tau/\lambda = 0.095$). We shall refer to this effect as diversification of the angular diffractal patterns. Thus, within the physical optics approximation, the scales of fractality manifest themselves (i.e. the scattering is effectively in the diffractal regime) only if the incident wavelength is sufficiently small. The simulations and the accompanying discussion presented at the end of section 2, indicate that the latter may not be an aftermath of the considered approximation. The small impact of the fractality scales on the propagating wave when the wavelength is large has also been observed in the problem of transmission trough Cantor-like slab [40]. We emphasize that this latter problem is treated with no approximation involved.

Since σ depends on the topothesy through $\hat{\tau}^{\sim D'/(1-D')}$, see (3.4), for type I surfaces and fixed D', the position of the peak is determined by the values of $\hat{\tau}$ alone. Figures 4(*a*) and 4(*b*) show $\cos\theta_{\text{ipeak}}$ versus the dimensionless topothesy $\hat{\tau}$, for $D_T = 1$ and $D_T = 2$, respectively. The curves correspond to: $D' = 0.1$, 0.2, 0.3, 0.4, 0.5, and 0.6, respectively from left to right. The onset of the curves marks the critical value $\hat{\tau}_c$ of the dimensionless topothesy for which the peak occurs. In particular, if $D' \ll 1$ (marginal fractals), using D' as a small parameter, one obtains

$$\cos\theta_{\text{ipeak}} \cong \frac{1}{\sqrt{2 + D_T}\hat{\tau}^{D'}} \tag{5.1}$$

which is valid to the leading order in D' and values of θ_{ipeak} away from normal incidence. The expression (5.1) appears similar to the analogous expression obtained using geometric optics for a Gaussian correlated surface with a steep RMS slope s, namely, $\hat{\tau}^{D'}$ substituted by s. However, the physical content of (5.1), being wavelength dependent, is different and furnishes an experimental possibility for measuring τ for marginal fractal surfaces.

Another special case are surfaces with dimension close to that of the Brownian fractal. Writing $D' = \frac{1}{2} \pm \eta$, and using η as a small parameter, for both $D_T = 1$ and $D_T = 2$, one

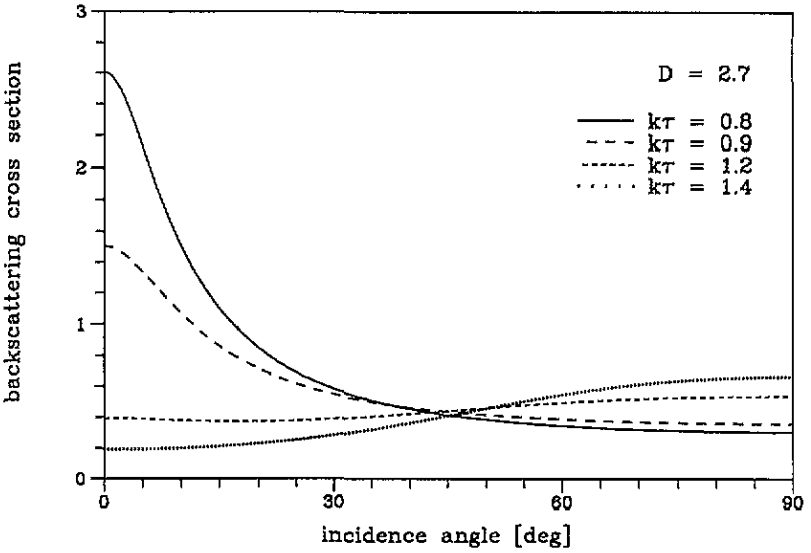

Figure 5. Backscattering diffractal patterns for pure fractal surfaces with $D = 2.7$. The full curve corresponds to $\hat{\tau} = 0.8$, the long dashes to $\hat{\tau} = 0.9$, short dashes to $\hat{\tau} = 1.2$, and the dotted curve to $\hat{\tau} = 1.4$.

gets

$$\cos\theta_{\text{ipeak}} \cong \frac{1}{\sqrt{2}\hat{\tau}^{D'/(1-D')}}. \tag{5.2}$$

This formula is a good approximation only for $\eta < 0.05$; for $D' = \frac{1}{2}$ it is exact and thus for Brownian surfaces $\hat{\tau}_c = 1/\sqrt{2}$. Again, the position of the peak depends on the value of the wavelength.

With increasing D', the interval of $\hat{\tau}$-values for which the peak exists becomes narrower and eventually disappears. The latter is illustrated in figure 5 where examples of diffractal angular patterns, type I surfaces are shown for $D = 2.7$. As we shall see in a moment the scattering from type I and type II surfaces are practically identical for this dimension. The full curve is drawn using $\hat{\tau} = 0.8$, the long dashes represent $\hat{\tau} = 0.9$, short dashes—$\hat{\tau} = 1.2$, and dotted curve—$\hat{\tau} = 1.4$. For these and higher values of the dimension, the diversification of the diffractal patterns manifests into a change from curves having maxima at zero and minima at $\pi/2$ to curves with reversed extrema.

Finally, we study the quantitative difference between the scattering form type I and type II surfaces. As already noted, this difference is negligible for large θ_i. Figure 6 shows the rate of decreasing of the relative difference $(\sigma_B^{II} - \sigma_B^{I})/\sigma_B^{I}$ with increasing dimensionless height, for fixed $\theta_i = 20°$ and $\hat{\tau} = 0.4$. The dimensions used to produce the curves are $D = 2.1, 2.2, 2.3, 2.4$, and 2.5; see the corresponding labels inside the figure. It is seen that the relative difference is significant, in some cases exceeding 100%, for fractal dimensions not much higher than D_T. With increasing D, $(\sigma_B^{II} - \sigma_B^{I})/\sigma_B^{I}$ rapidly decreases and for about $D' > 0.4$ it becomes negligible. To understand this, at first surprising fact, we rewrite $\tilde{k}_a^2$—see the argument of the hypergeometric function, equation (3.4)—in terms of D', D_T, θ_i and $\hat{h}$:

$$\tilde{k}_a^2 = \left[\frac{\Gamma(D_T + 1 - D')}{2^{1-2D'}\Gamma(D_T)\Gamma(D')}\frac{1}{\cos^2\theta_i \hat{h}^2}\right]^{1/(1-D')}.$$

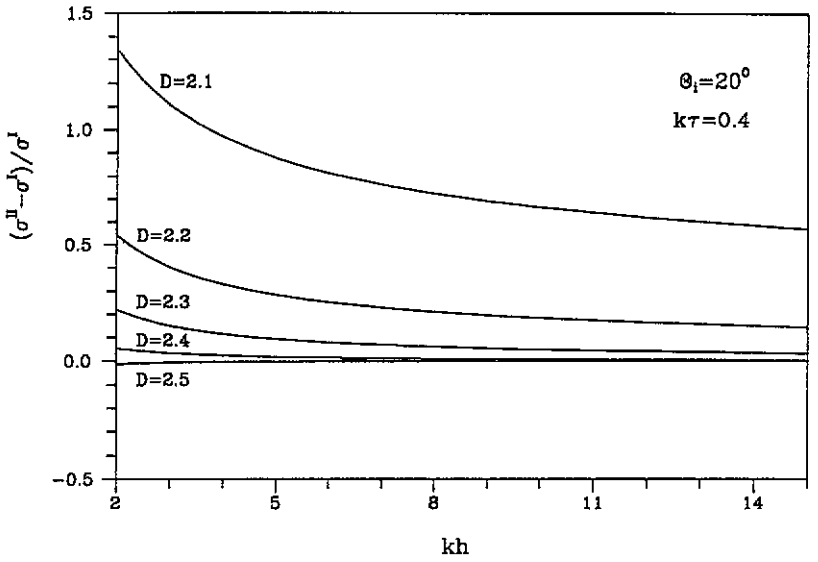

Figure 6. Relative difference between the backscattering cross section for type I and type II surfaces versus the dimensionless RMS height for fixed $\theta_i = 20°$ and $\hat{\tau} = 0.4$. The various curves correspond to fixed fractal dimensions; the values of the latter are given inside the figure.

Since the expression in the brackets is generally < 1, $\tilde{k}_a^2 \ll 1$ for $D' > 0.4$. Hence, ${}_1F_2 \cong 1$ and $\hat{\Delta}_{II}(u) \cong u^{2(1-D')}$ within the essential for the integration of (3.4) interval. On the other hand, if, as is usually the case for small and intermediate θ_i, $\hat{h} > 1/2\cos\theta_i$ the second exponent in the integrand of (3.4) is small. Therefore, according to the physical optics approximation, the scattering from type I and type II surfaces are closely similar for large and intermediate values of the fractal dimension excess.

6. Conclusions

We have studied some aspects of wave scattering from fractal rough surfaces. This problem constitutes an important example of so-called diffractal regime in wave theory [1]. Both pure fractal, i.e. surfaces having unbounded hierarchy of irregularities, and fractal surfaces with a largest possible scale have been considered. In the latter case an exact representation for the mean-square increment function is given. Within the framework of the physical optics (Kirchhoff) approximation, we have developed an elaborated combination of numerical and asymptotic technique which allows the evaluation of the incoherent scattering cross section (a quantity proportional to the second central moment of the scattered field) for any set of surface and scattering parameters. Using this technique, we have studied in detail the case of backscattering only. The emphasis is on the insight which the fractal parameters, such as dimension and topothesy, provide for analysing the diffractal phenomena.

The main finding is an effect of diversification of the angular diffractal patterns which takes place for wavelengths of the incident field below some critical value. In particular, the angular dependence of the backscattering cross section exhibits a peak at certain angles of incidence. The position of this peak and the critical wavelength are linked to the fractal dimension and the topothesy, and if confirmed experimentally, should furnish a precise method for measuring these intrinsic parameters of natural and man-made rough surfaces.

The peak occurs for fractal dimensions up to about 2.65; above this value, when the diffractal regime is in effect, the backscattered intensity has a maximum close to grazing incidence.

We have also quantified the impact which the largest scale of the surface has on the diffractal properties. For large angles of incidence this impact is negligible. For small and intermediate angles the effect is important only for relatively small excess of the fractal dimension over the topological one and decreases with increasing RMS height of the surface.

Acknowledgments

The authors thank N I Nickolaev for providing the simulation data used for figures 1 and 2, and for helpful discussions. This work was supported by Bulgarian Ministry of Science and Education, code F4.

Appendix. Type II mean-square increment function

In this appendix we sketch the steps leading toward expression (2.5). The derivation is based on the spectral representation of the MSI function [41]:

$$\Delta_{II}(\boldsymbol{r}_\perp) = 2\int_{-\infty}^{\infty}\left(1-\mathrm{e}^{-\mathrm{i}k_\perp\cdot r_\perp}\right)S_{II}(k_\perp)\frac{\mathrm{d}^{D_T}k_\perp}{(2\pi)^{D_T}}. \tag{A1}$$

Substituting (2.1) in (A1) (and employing polar coordinates for $D_T = 2$), (A1) can be brought to the following form:

$$\Delta_{II}(\xi) = \frac{2^{2-D_T}A_{II}}{\pi}\int_{k_a}^{\infty} k^{2D'-3}\begin{Bmatrix}1-\cos(k_a\xi)\\ 1-J_1(k_a\xi)\end{Bmatrix}\mathrm{d}k \qquad \begin{cases}D_T=1\\ D_T=2\end{cases} \tag{A2}$$

where ξ is either $|x|$ or $|\boldsymbol{r}_\perp|$. Next, the integral in (A2) is represented as $\int_{k_a}^{\infty} = \int_0^{\infty} - \int_0^{k_a}$. The first of these integrals is a representation of the MSI function for the pure fractal case; hence, it gives $\Delta_I(\xi)$—equation (2.3). The second integral is treated in the following manner: the oscillatory functions in the integrand are expanded in powers of $k_a\xi$ and the resulting series are integrated term-by-term; using the properties of the gamma function and the definition of the hypergeometric function, $\Delta_{II}(\xi)$ can be rearranged in the form of (2.5).

References

[1] Berry M V 1979 *J. Phys. A: Math. Gen.* **12** 781
[2] Mandelbrot B B 1977 *Fractals* (San Francisco: Freeman)
[3] Pietronero L and Tosatti E (eds) 1986 *Fractals in Physics* Amsterdam: North-Holland
[4] Sayles R S and Thomas T R 1978 *Nature* **271** 431
Berry M V and Hannay J H 1978 *Nature* **273** 573
[5] Pierson W J and Moskowitz L 1964 *J. Geophys. Res.* **69** 5181
[6] Bell T H 1978 *Deep-Sea Res.* A **26** 65
[7] Fuks I M 1983 *Radiophys. Quantum Electron.* **26** 865
[8] Ma Zhenyi *et al* 1991 *J. Mat. Res.* **6** 183
[9] Orey S 1970 *Z. Wahrsch'theorie verw. Geb.* **15** 249
[10] Berry M V and Blackwell T M 1981 *J. Phys. A: Math. Gen.* **14** 3101
[11] Jakeman E 1982 *J. Phys. A: Math. Gen.* **15** L55

[12] Yordanov O I 1990 *Proc. 6th Int. School on Microwave Physics and Technique (Varna)* ed A Y Spasov and M B Tsankov (Singapore: World Scientific) p 162
[13] Glazman R E and Weichman P B 1989 *J. Geophys. Res.* **94** 4998
[14] Falconer K J 1985 *The Geometry of Fractal Sets* (Cambridge: Cambridge University Press)
[15] Yordanov O I and Nickolaev N I 1994 Phys. Rev. E **49** R2517
[16] Mandelbrot B B 1982 *The Fractal Geometry of Nature* (San Francisco: Freeman)
[17] Osborne A R and Provinzale A 1989 Physica **35D** 357
[18] Greis N P and Greenside H S 1991 *Phys. Rev.* A **44** 2324
[19] Thorsos E I 1988 *J. Acoust. Soc. Am.* **83** 78
[20] Berry M V and Lewis Z V 1980 *Proc. R. Soc.* A **370** 459
[21] Po-zen Wong 1985 *Phys. Rev.* B **32** 7417
[22] Bass F G and Fuks I M 1979 *Wave Scattering from Statistically Rough Surfaces* (New York: Pergamon)
[23] Jackson D, Winebrenner D P and Ishimaru A 1988 *J. Acoust. Soc. Am.* **83** 961
[24] Thorsos E I and Jackson D R 1989 *J. Acoust. Soc. Am.* **86** 261
[25] Maue A W 1949 *Z. Phys.* **126** 601
[26] Meecham W C 1956 *J. Rat. Mech. Anal.* **5** 323
[27] Belobrov A V and Fuks I M 1985 *Sov. Phys. Acoust.* **31** 442
Rodriguez E 1989 *Radio Sci.* **24** 681
Ivanova K and Broschat S L 1993 *J. Acoust. Soc. Am.* **94** 2326
[28] Yordanov O I, Ivanova K and Michalev M A 1991 *J. Acoust. Soc. Am.* **89** 2104
[29] Lynch P J 1970 *J. Acoust. Soc. Am.* **47** 804
Shmelev A B 1972 *Soviet Phys. Usp.* **15** 173
Ogilvy J A 1987 *Rep. Prog. Phys.* **50** 1553
[30] Jackson D R, Winebrenner D P and Ishimaru A 1986 *J. Acoust. Soc. Am.* **79** 1410
[31] Dashen R, Henyey F S and Wurmser D 1990 *J. Acoust. Soc. Am.* **88** 310
[32] Kravtzov Yu A, Fuks I M and Shmelev A B 1971 *Izv. Vysshih. Uchebnih. Zavedenia Radiofizika* **14** 854
Lysanov Y P 1971 *Soviet Phys. Acoust.* **17** 74
[33] Yordanov O I and Michalev M A 1989 *J. Opt. Soc. Am.* A **6** 1578
[34] Yordanov O I and Stoyanov O 1989 *Proc. URSI Int. Symp. on EM Theory (Stockholm)* (Stockholm: The Royal Institute of Technology) p 512
[35] Ishimaru A 1978 *Wave Propagation and Scattering in Random Media* (New York: Academic Press)
[36] Prudnikov A P, Brichkov Yu A and Marichev O I 1986 *Integrals and Series* (New York: Gordon and Breach)
[37] Bender C M and Orszag S A 1978 *Advanced Mathematical Methods for Scientists and Engineers* (New York: McGraw-Hill)
[38] Abramowitz M and Stegun I A 1970 *Handbook of Mathematical Functions* (New York: Dover)
[39] Handelsman R A and Lew J S 1969 *Arch. Rational. Mach. Anal.* **35** 382
Bleistein N 1977 *SIAM J. Math. Anal.* **8** 655
Soni K 1980 *SIAM J. Math. Anal.* **11** 828
[40] Konotop V V, Yordanov O I and Yurkevich I V 1990 *Europhys. Lett.* **12** 481
[41] Panchev S 1971 *Random Functions and Turbulence* (Oxford: Pergamon)